Batteries & Supercaps

Research Article
doi.org/10.1002/batt.202200386

Chemistry Europe
European Chemical Societies Publishing

www.batteries-supercaps.org

Two-Electron Tetrathiafulvalene Catholytes for Nonaqueous Redox Flow Batteries

Nicolas Daub,[a] Koen H. Hendriks,[a, b] and René A. J. Janssen*[a, b]

Tetrathiafulvalene (TTF) exhibits two reversible oxidation steps and is used as a novel multi-electron catholyte for nonaqueous organic redox flow batteries. To increase solubility in polar organic solvents, TTF derivatives with polar side chains are synthesized. 4-Methoxymethyltetrathiafulvalene emerges as a promising two-electron catholyte because it is a liquid at room temperature and miscible with acetonitrile. Bulk-electrolysis experiments and UV-vis-NIR absorption spectroscopy reveal excellent cycling stability for the first and second electrochemical oxidations. In the doubly oxidized state, the TTF derivatives show a reversible about 1% loss of the state of charge per day, due to extrinsic effects. In a symmetric redox flow battery, 4-methoxymethyltetrathiafulvalene shows a volumetric capacity loss of only 0.2% per cycle with a Coulombic efficiency (CE) of 99.6%. In an asymmetric redox flow battery with a pyromellitic diimide as two-electron anolyte, the capacity loss is 0.8% per cycle, with CE > 99% in each cycle.

Introduction

Redox flow batteries (RFBs) can provide effective large scale storage of surplus renewable energy and prevent the power grid from overloading.[1–4] Conventional RFBs are based on Fe/Cr, Zn/Br, or V/VO redox couples and use aqueous media for operation.[5,6] In recent years there is considerable interest in RFBs based on organic anolytes and catholytes[7–13] to circumvent some of the drawbacks associated with inorganic materials in terms of environmental concerns or lack of earth-abundancy. Organic RFBs can be aqueous or nonaqueous. Nonaqueous RFBs operate with organic solvents which allow for a much wider, up to three times, potential window than water.[14] Preferably, organic catholytes and anolytes for nonaqueous RFBs are low-molecular weight ($M < 150\ g\,mol^{-1}$) compounds that are highly soluble in polar organic solvents and stable in their neutral, and oxidized and reduced states. Compared to redox-active molecules that feature a single redox event,[15–28] molecules that sustain multiple redox steps can increase volumetric capacity.[29–47] Importantly, this should not go at the cost of solubility and stability, and their design is a subtle challenge. So far, few catholytes with stable double oxidation for use in nonaqueous RFBs have been described. Structural motifs used for twofold oxidation are phenazines,[34,36] phenothiazine,[31,37] and diaminoanthraquinones,[29,39] next to hybrid diaminocyclopropenium-phenazine/phenothiazine[42,43] and oligomeric catholytes, e.g., based on cyclopropenium[38] or ferrocene.[32,46] Only few of these have sufficient solubility (Table S1, Supporting Information) for practical application.[48] The use of multi-redox materials can lead to a variable output voltage as a function of the state-of-charge or discharge rate.

Here, we investigate tetrathiafulvalene (TTF) (**1**, Figure 1) as two-electron catholyte for use in nonaqueous organic RFBs. TTF is a well-known electron donor that is readily oxidized in two consecutive one-electron oxidations.[49] TTF has been used a redox mediator to enhance the recharging rate of non-aqueous Li–O_2 batteries[50,51] and as component in an organic electrode material,[52,53] but so far has not been evaluated for RFB applications.[54] To enhance solubility in acetonitrile, TTF was derivatized with different polar side chains (**1**–**4**, Figure 1). Bulk-electrolysis and UV-vis-NIR spectroscopy revealed good cycling stability and shelf-life in the doubly oxidized state for the TTF derivates tested. Because of its high solubility, **2** was evaluated in a symmetric single-component flow-battery cycling experiment using its radical cation $\mathbf{2}^{+\bullet}$ as amphoteric redox active species in anolyte ($e^- + \mathbf{2}^{+\bullet} \rightleftarrows \mathbf{2}$) and catholyte ($\mathbf{2}^{+\bullet} \rightleftarrows \mathbf{2}^{2+} + e^-$) compartments. Under these conditions the battery is very stable, exhibiting a Coulombic efficiency (CE) of 99.6% and a volumetric capacity decay of less than 0.2% per cycle. In combination with pyromellitic diimides as two-electron anolyte,[45] two-electron catholyte **2** is somewhat less stable and provides a capacity loss of 0.8% per cycle with CE > 99%. The reduced capacity results from crossover of the catholyte through the anion exchange membrane.

Results and Discussion

Unsubstituted TTF (**1**) exhibits two reversible oxidations (Figure 2a) but has limited solubility (0.25 ± 0.005 M) in acetonitrile (Table S2, Supporting Information), i.e., about one order of

[a] N. Daub, Dr. K. H. Hendriks, Prof. R. A. J. Janssen
Molecular Materials and Nanosystems & Institute for Complex Molecular Systems
Eindhoven University of Technology
PO Box, 5600 MB Eindhoven, The Netherlands
E-mail: r.a.j.janssen@tue.nl
[b] Dr. K. H. Hendriks, Prof. R. A. J. Janssen
Dutch Institute for Fundamental Energy Research
De Zaale 20, 5612 AJ Eindhoven, The Netherlands

Supporting information for this article is available on the WWW under https://doi.org/10.1002/batt.202200386

Research Article
doi.org/10.1002/batt.202200386
Chemistry Europe
European Chemical Societies Publishing

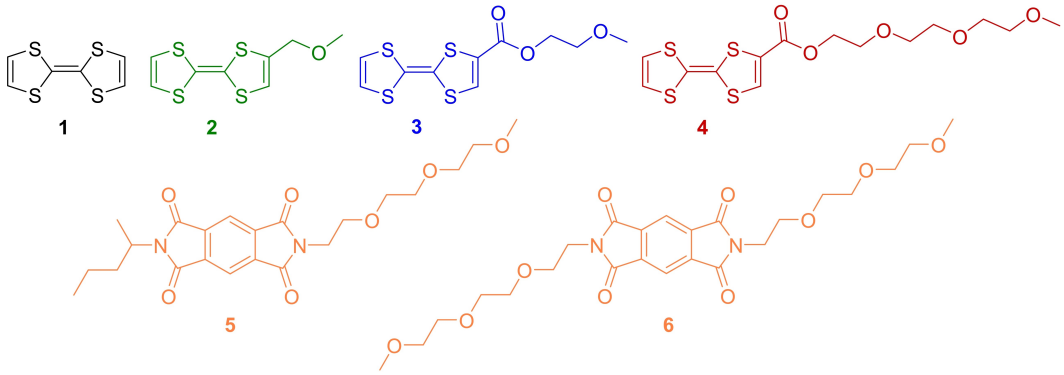

Figure 1. Structure of two-electron TTF catholytes **1**–**4** and two-electron pyromellitic diimide anolytes **5, 6**.

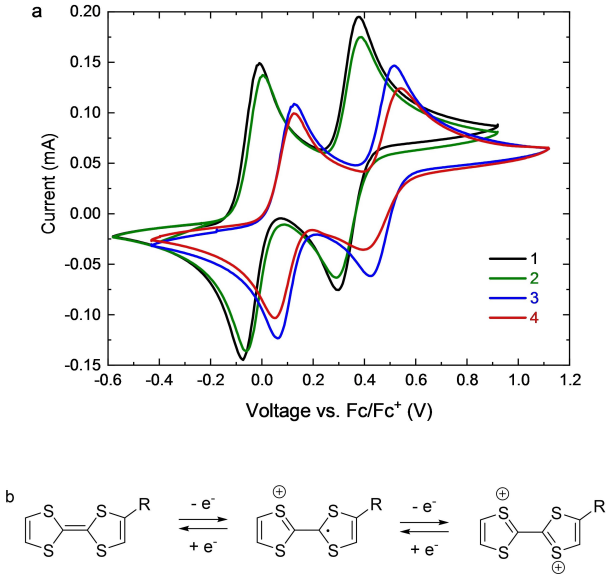

Figure 2. a) Cyclic voltammograms of **1**–**4** (5 mM in acetonitrile containing 200 mM $TBAPF_6$) recorded with a scan rate of 100 $mV\,s^{-1}$. b) The two one-electron oxidation reactions of tetrathiafulvalene derivatives.

magnitude below requirements for practical applications.[48] To enhance solubility, a methylmethoxy-substituted TTF derivative (**2**) was synthesized. Lithiation of TTF, followed by formylation with *N*-methylformanilide and quenching with 1 M HCl resulted in 4-formyltetrathiafulvalene (Scheme S1, Supporting Information). Reduction of the latter with $NaBH_4$, followed by methylation with iodomethane gave 4-methoxymethyltetrathiafulvalene (**2**) which is a liquid at room temperature with a molarity of 6 ± 0.2 M (Table S2, Supporting Information). To increase the oxidation potential, while keeping high solubility, ester-functionalized TTF derivatives (**3** and **4**) were synthesized by lithiation of TTF, followed by quenching with the corresponding acid chloride (Scheme S1, Supporting Information). While **3** is a solid with a solubility of 0.17 ± 0.01 M in acetonitrile, **4** is a liquid at room temperature that is completely miscible with acetonitrile and has a molarity of 3.8 ± 0.2 M (Table S2, Supporting Information). Detailed synthetic procedures and characterization with NMR and mass spectrometry are described in the Supporting Information.

Anolytes *N*-2-pentyl-*N*′-2-(2-(2-methoxyethoxy)ethoxy)ethylaminepyromellitic diimide (**5**) and N,N′-bis(2-(2-(2-methoxyethoxy)ethoxy)ethylaminepyromellitic diimide) (**6**) were synthesized as described before.[45]

Cyclic voltammetry (CV) was performed to determine the oxidation potentials of **1**–**4** and their kinetic and chemical reversibility in dilute solutions (Figure 2a and Table 1).

Compounds **1**–**4** each exhibit two quasi-reversible redox waves corresponding to two one-electron oxidation steps to the radical cation and the dication (Figure 2b). Compared to **1** and **2**, the oxidation potentials of **3** and **4** have shifted anodically by 0.11–0.14 V due to the carboxylic ester substitution. Except for **1**, the chemical reversibility of the second oxidation wave inferred from the i_{pc}/i_{pa} peak current ratio seems to be less than for the first oxidation. However, increasing the scan rate results in a further reduction of i_{pc}/i_{pa} (Figure S1, Supporting Information). The reduction of i_{pc}/i_{pa} at higher scan rates is accompanied by broadening of the re-reduction of the second oxidation wave, resulting in a larger peak separation. This indicates that the second oxidation and the corresponding re-reduction are kinetically hampered, but not necessarily lead to chemical instabilities.

Density functional theory (DFT) calculations have shown that neutral TTF (**1**) adopts a C_{2v} (boat-like) conformation with a short (1.349 Å) bond linking the two rings.[55] The $TTF^{+\bullet}$ cation radical ($\mathbf{1}^{+\bullet}$) is planar (D_{2h}) with an elongated (1.396 Å) inter-ring bond while the TTF^{2+} ($\mathbf{1}^{2+}$)dication adopts a D_2 structure in which the two rings are planar but twisted around a long (1.454 Å) central bond by an angle of 35.9°.[55] Electron spin

Table 1. Oxidation potentials and peak ratios of the CVs of **1**–**4** shown in Figure 2.

		$E_{1/2}$ vs Fc/Fc^+ [V]	$\bar{E}_{1/2}$ vs Fc/Fc^+ [V]	i_{pc}/i_{pa}
1	1st	−0.04	+0.15	0.99
	2nd	+0.34		0.95
2	1st	−0.02	+0.16	1.04
	2nd	+0.34		0.88
3	1st	+0.09	+0.29	1.01
	2nd	+0.48		0.88
4	1st	+0.09	+0.28	0.96
	2nd	+0.47		0.87

Research Article
doi.org/10.1002/batt.202200386
Chemistry Europe
European Chemical Societies Publishing

resonance spectroscopy confirms that all four H atoms of the $TTF^{+\bullet}$ cation radical are identical.[56] The two rings each possess 6π electrons in $\mathbf{1}^{2+}$ and are thus aromatic, evidenced by the significant downfield shift of the ^{1}H NMR signal from $\delta_H = 6.44$ to 9.51 ppm in CD_3CN when going from **1** to $\mathbf{1}^{2+}$.[57] For the substituted TTF derivatives (**2**–**4**) the charge distribution in the charged state is likely asymmetric. For **3** and **4** the positive charge is expected to be more on the non-substituted dithiole ring as a consequence of the electron withdrawing carboxylic ester substituent.

CV was used to determine the diffusion coefficients (*D*) via the Randles-Ševčik equation and the heterogenous electron transfer rates (k_0) following the Nicholson method (Figures S2 and S3, and Table S3, Supporting Information).[58,59] In agreement with the Stokes-Einstein relation *D* decreases with increasing molecular size. The values obtained for *D* and k_0 are higher than for most of molecules considered appropriate for RFB applications.[60,61]

Bulk electrolysis cycling was performed to evaluate the stability of molecules **1**–**4** in the oxidized state and their cyclability. Representative two-electron charge and discharge capacities of the four TTF derivatives reveal a near-linear capacity loss per cycle (Figure 3). Compounds **1** and **2** exhibit a decay over the first 150 cycles of about 0.4% per cycle, while **3** and **4** degrade slower, by about 0.2%–0.3% per cycle. The charge/discharge capacity of **2** is the highest initially but it degrades faster per cycle. TTF derivative **4** has the lowest utilization. When plotted versus time **1**, **2**, and **4** show very similar decay of 1.1–1.3% h^{-1} within the first 40 h, while **3** degrades less (0.7% h^{-1}) (Figure S4 and Table S4, Supporting Information). Investigation of the stabilities of the individual $\mathbf{2} \rightleftarrows \mathbf{2}^{+\bullet}$ and $\mathbf{2}^{+\bullet} \rightleftarrows \mathbf{2}^{2+}$ redox steps **in** bulk electrolysis showed that the capacity fades of the two one-electron charge-discharge processes are very similar and similar to that of the two-electron $\mathbf{2} \leftrightarrow \mathbf{2}^{2+}$ process (Figure S5 and Table S4, Supporting Information). This shows that stability is independent of the specific state of charge (either $\mathbf{2}^{+\bullet}$ or $\mathbf{2}^{2+}$). The capacity decay recorded at varying charge-discharge currents revealed slower degradation per cycle when charging and discharging faster

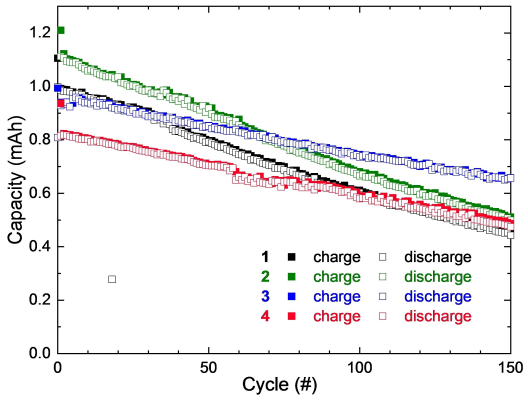

Figure 3. Charge and discharge capacity versus cycle number for a two-electron charge-discharge bulk electrolysis in a H-cell containing 5 mM of **1**–**4** in acetonitrile containing 200 mM $TABPF_6$.

(Figure S6 and Table S5, Supporting Information). This suggests that under these conditions the degradation is time-dependent.

To examine the stability in the oxidized state in more detail, UV-vis-NIR absorption spectra of 5 mM solutions of **1**–**4** in acetonitrile containing 200 mM of $TBAPF_6$ were recorded at various state-of-charge (SOC) during the oxidation process (Figure 4). In the neutral state (0% SOC) TTF derivatives **1**–**4** show main absorption bands at 313–316 nm and low-intensity peaks at 445–450 nm for **1** and **2** and at 431 nm for **3** and **4**. When oxidized to the $TTF^{+\bullet}$ radical cations (50% SOC) a series of new peaks and shoulders appear in each case. The $TTF^{+\bullet}$ radical cations exhibit a strong absorption at 430–440 nm, accompanied by less intense peaks maximizing at 335–345 and 565–580 nm. These bands agree well with spectra previously reported for $TTF^{+\bullet}$ radical cations.[62] In addition, a broad, low-intensity absorption are observed in the near infrared region between 750 and 770 nm, assigned to the charge transfer band of $(TTF^{+\bullet})_2$ dimers.[62–64] The interconversion from the neutral TTF compounds to the $TTF^{+\bullet}$ radical cations is accompanied by isosbestic an point at 333 nm. Upon further oxidation, TTF^{2+} dications (100% SOC) are formed. The TTF^{2+} dications exhibit two peaks. The most intense peaks for TTF^{2+} are found at 353–357 nm for **1**, **3**, and **4** and at 370 nm for **2**. The second peak is at 272–276 nm.[65] Also the conversion of the $TTF^{+\bullet}$ radical cation to the TTF^{2+} dication is accompanied by a an isosbestic point, found at 290 nm for **1**, **3**, and **4** and at 397 nm for **2**.

UV-vis-NIR absorption spectroscopy was used to monitor the stability of the TTF^{2+} dications in acetonitrile with time. Importantly, the TTF derivatives do not degrade, but rather the dications are re-reduced to the radical cations as evidenced by the appearance of the $TTF^{+\bullet}$ spectra and isosbestic points (Figure S7, Supporting Information). No additional new peaks are found except for a very small peak at 308 nm for **4**. Because the main peaks in the UV-vis-NIR absorption spectra of the TTF^{2+} dications overlap with those of the $TTF^{+\bullet}$ radical cations, it is more accurate to determine the stability of the TTF^{2+} dications from the formation of $TTF^{+\bullet}$. The SOC of the TTF^{2+} dications of **1**–**4**, monitored over the course of for 37 days at two different wavelengths for the formation of $TTF^{+\bullet}$ (Figure 5), reveals a very good stability. The loss in SOC is less than 1% per day, with **2** being the least and **1** the most stable derivative. The nature of the species that reduces the TTF^{2+} dications under these conditions is not known. It might be a contamination in the electrolyte or the acetonitrile itself.

Figures 4 and 5 indicate that each of the molecules **1**–**4** exhibits good cyclability and stability. Of the four TTF derivatives compound **2** has the highest molarity of 6 M and is miscible with acetonitrile. After isolating the $\mathbf{2}^{2+}(PF_6^-)_2$ salt, its solubility in acetonitrile was determined to be 1.4 ± 0.2 M (Table S2, Supporting Information) corresponding to a theoretical volumetric capacity of 75 Ah L^{-1} when used in a redox flow battery. This makes **2** an excellent candidate for use in an organic RFB.

To investigate the stability of **2** at increased concentration under more realistic RFB conditions a single-compound cycling experiment was carried out at 50 mM concentration in a

Research Article
doi.org/10.1002/batt.202200386
Chemistry Europe
European Chemical Societies Publishing

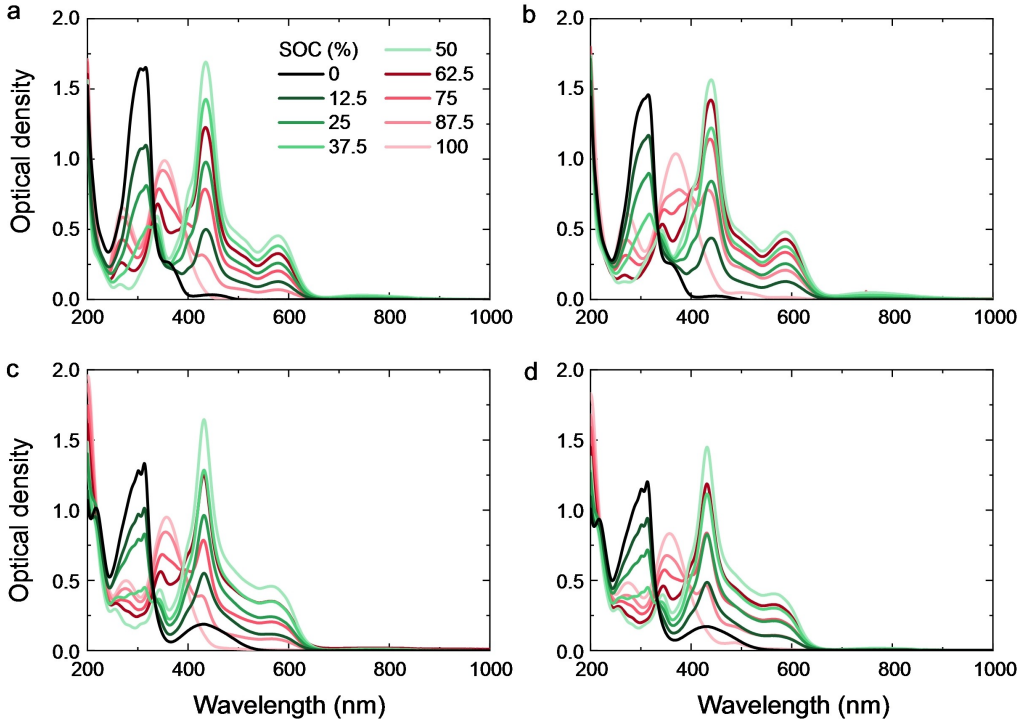

Figure 4. UV-vis-NIR absorption spectra at different SOC of 5 mM solutions of TTF derivatives in acetonitrile containing 200 mM $TBAPF_6$. a) **1**, b) **2**, c) **3** and d) **4**. Black lines represent the neutral compounds, green lines the stepwise electrochemical oxidation to 50% SOC ($TTF^{+\bullet}$, singly oxidized), and red lines the stepwise electrochemical oxidation from 50% to 100% SOC (TTF^{2+}, doubly oxidized). The spectra were recorded directly after reaching the SOC.

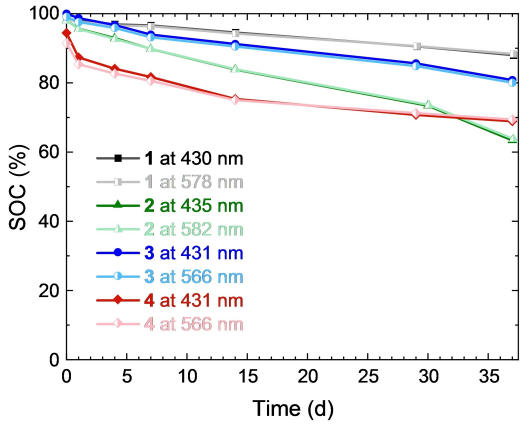

Figure 5. Retention of the SOC of double-oxidized solutions of electrochemically charged 5 mM solutions of the compounds **1**–**4** in acetonitrile containing 200 mM of $TBAPF_6$.

prototype flow setup. For this purpose, a 50 mM acetonitrile solution of doubly-oxidized **2** containing 1-ethyl-3-methylimidazolium hexafluorophosphate ($EMIMPF_6$) as electrolyte was prepared via bulk electrolysis. The fully oxidized solution was then mixed with an equal amount of a solution of neutral **2** of the same concentration, solvent, and electrolyte salt, yielding a starting solution at 50% SOC. This solution was equally divided over the compartments of the prototype flow battery. By applying a positive current over the electrodes of the battery (positive polarization), the solution in one compartment is re-reduced towards 0% SOC while the other one is further oxidized towards 100% SOC. Applying a negative current (negative polarization) results in reversal of the SOC between the compartments. This represents one cycle. Because **2** is cycled between neutral and dicationic states, an anion exchange membrane was used. Amongst various anion exchange membranes, a Fumasep FAA-3-50 proved to be suitable for the single-compound flow cycling experiment. During 3 days of cycling a capacity loss of only 0.2% per cycle and 3.1% per day was observed, while the Coulombic efficiency (CE) remained 99.6% (Figure 6a). Also, the voltage versus time curves show the expected behavior (Figure 6b). The charging and discharging curves are symmetrical to the abscissa. The oxidation from neutral to singly-oxidized, respectively from singly- to doubly-oxidized occur at $\pm$50 mV and $\pm$450 mV and thus show only a low overpotential of 50 mV. This demonstrates the good stability as well as cyclability of **2** in cycling between neutral, singly-oxidized, and doubly-oxidized states.

The capacity fade in the symmetric RFB of 3.1% per day is much smaller than found in the bulk electrolysis experiments in a H-cell (1.15% per hour). In contrast to the RFB, the potential at the counter electrode in the bulk electrolysis is determined by the applied charge/discharge current and was found to vary between 6 and 10 V in several independent measurements. The highly negative potential will lead to reactive species that make the bulk electrolysis system degrade faster. In the symmetric RFB the maximum applied potential is only $+$0.6 V or $-$0.6 V (Figure 6). Hence the 3.1% per day decay seen in the symmetric flow cell is a more realistic estimate for what can be achieved in a RFB. The capacity loss of 3.1% per day implies that under

Research Article
doi.org/10.1002/batt.202200386
Chemistry Europe
European Chemical Societies Publishing

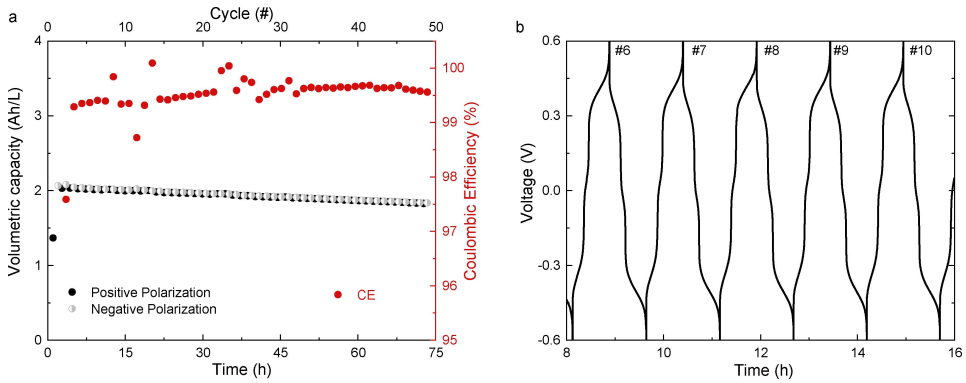

Figure 6. a) Charge-discharge capacity and Coulombic efficiency versus time and cycle number for a symmetric flow battery, cycling with 50 mM of $\mathbf{2}^{+\bullet}$ in acetonitrile containing 200 mM $EMIMPF_6$ using a Fumasep FAA-3-50 membrane anion exchange membrane. b) Voltage versus time curves of the cycles 6 to 10.

RFB conditions the stability of the redox system is less than the intrinsic stability of the TTF^{2+} dications of 1% as determined from UV-vis-NIR experiments (Figure 5). Hence, the intrinsic stability of the TTF^{2+} dications is not the prime cause of the capacity fade. The capacity fade may be dominated by cross-over of redox species or their interaction with the electrodes.

Surprisingly, mixtures of TTF **2** as catholyte and pyromellitic diimide **5** as anolyte[45] in acetonitrile are greenish, while the catholyte solution is yellow and the anolyte solution is colorless. UV-vis-NIR measurements of mixed anolyte and catholyte at different concentrations revealed the formation of a charge-transfer complex between **2** as donor and **5** as acceptor that exhibits a charge-transfer band at 595 nm (Figure 7). A bimolecular association model fitted to the data, using a non-linear least-squares fit (Figure S8)[66] resulted in $\varepsilon = 420 \pm 60\ cm^{-1}M^{-1}$ for the molar absorption coefficient at 595 nm and $K_a = 1.3 \pm 0.3\ M^{-1}$ for the association constant of this charge-transfer complex. The shape of the charge-transfer absorption band is independent of the concentration (Figure 7), consistent with formation of a 1:1 complex. Further evidence of a 1:1 association is obtained from a Job plot (Figure S9). We assume

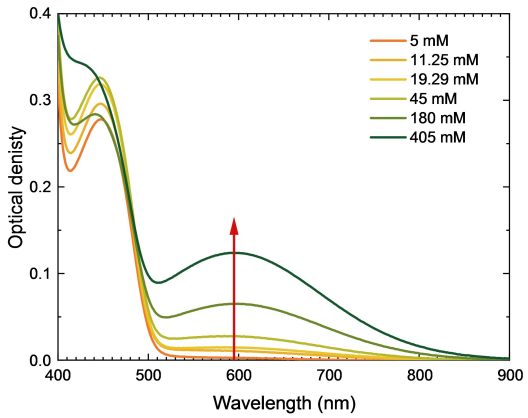

Figure 7. UV-vis-NIR measurements of a 45 mM solution of TTF **2** in acetonitrile containing 200 mM $TBAPF_6$ containing different concentrations of diimide **5** used to determine K_a and ε. The charge-transfer absorption band at 595 nm is indicated with a red arrow.

that formation of the charge-transfer complex between **2** and **5** hinders a mixed flow battery from charging and discharging properly.

A non-mixed RFB was used to assess TTF derivative **2** as two-electron catholyte at 50 mM concentration using 50 mM pyromellitic diimides (**5** and **6**) as two-electron anolytes in acetonitrile containing $TBAPF_6$ as electrolyte salt. A more selective Fumasep FAPQ-375-PP anion exchange membrane was used to slow down crossover of redox species. For the **2**/**5** battery (Figure 8) two membrane layers were stacked, while for **2**/**6** battery (Figure S10, Supporting Information) one layer was used. Both RFBs were galvanostatically cycled at 5 $mA\,cm^{-2}$ and reached a utilization of 96%, respectively 84%, showing that the additional membrane layer limits the utilization. As this value is highly dependent on the current, a combined constant current and voltage cycling could be used in order to increase this. Figure 8a shows that the capacity of the redox flow battery drops in the first 70 cycles to 46% of its initial value, representing a 0.8% loss per cycle, corresponding to 12% per day when cycled continuously, while the Coulombic efficiency of each cycle remains close to 99%. Analyzing the CVs of the catholyte and anolyte solutions of the **2**/**5** battery prior to and after 4.5 days of cycling, and correcting for solvent transfer from anolyte to catholyte reservoirs, reveals a 56% loss of **2** at the catholyte side. This correlates well with the 54% loss in discharge capacity. While catholyte **2** is almost equally spread over both reservoirs, anolyte **5** mostly remained in its initial reservoir (Figure 8b). In addition, some of TTF **2** might have degraded, which is inferred from the fact that summing up the i_{pa} of the catholyte signals in the CVs after of both reservoirs adds up to only 86%. The loss of redox active compound (~3% per day) in the **2**/**5** RFB is very similar to the loss of **2** in the single-compound RFB shown in Figure 6 (~3% per day). This decay could be a result of the interaction of the active materials with the carbon electrode while charging and discharging, as a charged solution of the catholyte itself does not degrade when being stored separately (Figure S7, Supporting Information). Furthermore, a slow increase of the area-specific resistivity (ASR) was seen from about 66 to 71 $\Omega\,cm^2$ after cycling which is tentatively attributed to membrane degradation (Figure S11,

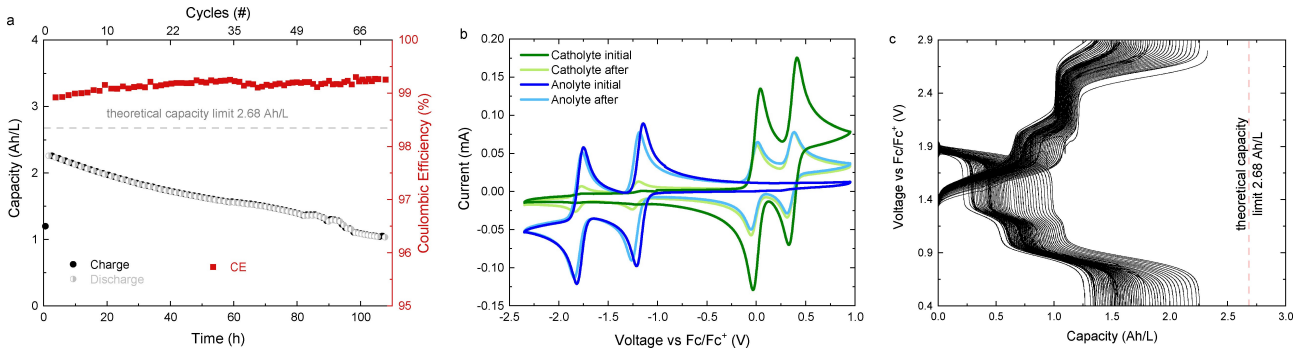

Figure 8. a) Charge-discharge capacity and Coulombic efficiency versus time and cycle number for a non-mixed flow battery, cycling with 50 mM catholyte **2** and 50 mM anolyte **5**, both in acetonitrile containing 300 mM $TBAPF_6$, using two layers of a Fumasep FAPQ-375-PP anion exchange membrane. b) CVs before and after flow cycling for 4.5 days shown in (a). The CVs were corrected for 0.5 mL solvent transfer from anolyte to catholyte. c) Voltage versus volumetric capacity curves.

Supporting Information). The Coulombic efficiency reached 99.3%. Figure 8(c) shows the voltage versus volumetric capacity.

For the **2**/**6** RFB essentially similar results were found (Figure S10, Supporting information) with a total loss of about 12% per day during the first three days and a Coulombic efficiency of >98% on average. In both RFBs (**2**/**5** and **2**/**6**) the catholyte (**2**) crosses over faster than the anolyte (**5**/**6**). Immersing the anion exchange membrane into acetonitrile leads to visible swelling and likely causes the formation of percolation pathways thatsustain the diffusion of anolyte and catholyte molecules. Because of its smaller size, the crossover of the catholyte is faster. At present it is not known if the crossover rate depends on the SOC.

Cycling all-organic RFBs with TTF **2** at higher concentrations was severely limited by capacity loss due to unwanted crossover. At higher concentration the catholyte already crosses over during the first cycle and forms the charge transfer complex. To render high concentration cycling possible, improved membrane separators are needed or TTF derivatives with less membrane permeability.

Conclusion

TTF derivatives have been identified as a new class of multi-electron catholyte for nonaqueous RFBs. Increasing the number of redox events per molecule is a strategy to increase the charge density. By optimizing the solubility via the use of polar side chains, a molarity of 6 M was achieved for TTF derivative **2** and a solubility of 1.4 M for the dicationic $\mathbf{2}^{2+}(PF_6^-)_2$ salt. UV-vis-NIR spectroscopy showed that singly and doubly oxidized TTF derivatives in electrolyte solutions exhibit good intrinsic shelf-life stability and good cyclability in bulk electrolysis. A single-compound redox flow cycling (between $\mathbf{2}^{+\bullet} \rightleftarrows \mathbf{2}$ and $\mathbf{2}^{+} \rightleftarrows \mathbf{2}^{2+}$) showed a decay of less than 0.2% per cycle at a current of 5 mA cm^{-2}. The formation of a charge-transfer complex of TTF **2** with diimide **5** precluded the use of **2** and **5** in a mixed RFBs. A proof-of-principle non-mixed RFB using TTF **2** and diimide **5** or **6** as multi-electron anolytes as catholytes revealed a high Coulombic efficiency (>99%) and a decay of 0.8% per cycle, primarily caused by a limited selectivity of the membrane.

Acknowledgements

We thank Stefan Meskers for helpful discussions. We acknowledge funding from the Eindhoven University of Technology, the Dutch Research Council (NWO) (016.VENI.182.006 and Spinoza grant), and the Ministry of Education, Culture and Science (Gravity program 024.001.035).

Conflict of Interest

The authors declare no conflict of interest.

Data Availability Statement

The data that support the findings of this study are available from the corresponding author upon reasonable request.

Keywords: catholyte · charge transfer complex · multi electron · nonaqueous redox flow battery · tetrathiafulvalene

[1] G. L. Soloveichik, Flow *Chem. Rev.* **2015**, *115*, 11533–11558.
[2] M. Park, J. Ryu, W. Wang, J. Cho, *Nat. Rev. Mater.* **2017**, *2*, 16080.
[3] T. Shigematsu, *Curr. Opin. Electrochem.* **2019**, *18*, 55–60.
[4] E. Sanchez-Diez, E. Ventosa, M. Guarnieri, A. Trovo, C. Flox, R. Marcilla, F. Soavi, P. Mazur, E. Aranzabe, R. Ferret, *J. Power Sources* **2021**, *481*, 228804.
[5] J. Noack, N. Roznyatovskaya, T. Herr, P. Fischer, *Angew. Chem. Int. Ed.* **2015**, *54*, 9776–9809; *Angew. Chem.* **2015**, *127*, 9912–9947.
[6] R. K. Emmett, M. E. Roberts, *J. Power Sources* **2021**, *506*, 230087.
[7] J. Winsberg, T. Hagemann, T. Janoschka, M. D. Hager, U. S. Schubert, *Angew. Chem. Int. Ed.* **2017**, *56*, 686–711; *Angew. Chem.* **2017**, *129*, 702–729.
[8] X. Wei, W. Pan, W. Duan, A. Hollas, Z. Yang, B. Li, Z. Nie, J. Liu, D. Reed, W. Wang, V. Sprenkle, *ACS Energy Lett.* **2017**, *2*, 2187–2204.

[9] P. Leung, A. A. Shah, L. Sanz, C. Flox, J. R. Morante, Q. Xu, M. R. Mohamed, C. Ponce de León, F. C. Walsh, *J. Power Sources* **2017**, *360*, 243–283.
[10] H. Chen, G. Cong, Y.-C. Lu, *J. Energy Chem.* **2018**, *27*, 1304–1325.
[11] Y. Ding, C. Zhang, L. Zhang, Y. Zhou, G. Yu, *Chem. Soc. Rev.* **2018**, *47*, 69–103.
[12] J. Luo, B. Hu, M. Hu, Y. Zhao, T. L. Liu, *ACS Energy Lett.* **2019**, *4*, 2220–2240.
[13] J. Chai, A. Lashgari, J. Jiang, *ACS Symp. Ser.* **2020**, *1364*, 1–47.
[14] K. Gong, Q. Fang, S. Gu, S. S. F. Y. Li, Y. Yan, *Energy Environ. Sci.* **2015**, *8*, 3515–3530.
[15] J. Huang, L. Cheng, R. S. Assary, P. Wang, Z. Xue, A. K. Burrell, L. Curtiss, L. Zhang, *Adv. Energy Mater.* **2015**, *5*, 1401782.
[16] X. Wei, W. Xu, J. Huang, L. Zhang, E. Walter, C. Lawrence, M. Vijayakumar, W. A. Henderson, T. Liu, L. Cosimbescu, B. Li, V. Sprenkle, W. Wang, *Angew. Chem. Int. Ed.* **2015**, *54*, 8684–8687; *Angew. Chem.* **2015**, *127*, 8808–8811.
[17] J. D. Milshtein, A. P. Kaur, M. D. Casselman, J. A. Kowalski, S. Modekrutti, P. L. Zhang, N. H. Attanayake, C. F. Elliott, S. R. Parkin, C. Risko, F. R. Brushett, S. A. Odom, *Energy Environ. Sci.* **2016**, *9*, 3531–3543.
[18] X. Wei, W. Duan, J. Huang, L. Zhang, B. Li, D. Reed, W. Xu, V. Sprenkle, W. Wang, *ACS Energy Lett.* **2016**, *1*, 705–711.
[19] M. Milton, Q. Cheng, Y. Yang, C. Nuckolls, R. Hernández Sánchez, T. J. Sisto, *Nano Lett.* **2017**, *17*, 7859–7863.
[20] W. Duan, J. Huang, J. A. Kowalski, I. A. Shkrob, M. Vijayakumar, E. Walter, B. Pan, Z. Yang, J. D. Milshtein, B. Li, C. Liao, Z. Zhang, W. Wang, J. Liu, J. S. Moore, F. R. Brushett, L. Zhang, X Wei, *ACS Energy Lett.* **2017**, *2*, 1156–1161.
[21] G. Wang, B. Huang, D. Liu, D. Zheng, J. Harris, J. Xue, D. Qu, *J. Mater. Chem. A* **2018**, *6*, 13286–13293.
[22] M. J. Baran, M. N. Braten, E. C. Montoto, Z. T. Gossage, L. Ma, E. Chénard, J. S. Moore, J. Rodríguez-López, B. A. Helms, *Chem. Mater.* **2018**, *30*, 3861–3866.
[23] C. Zhang, Z. Niu, Y. Ding, L. Zhang, Y. Zhou, X. Guo, X. Zhang, Y. Zhao, G. Yu, *Chem* **2018**, *4*, 2814–2825.
[24] J. Yuan, C. Zhang, Y. Zhen, Y. Zhao, Y. Li, *J. Power Sources* **2019**, *443*, 227283.
[25] Y. Yan, S. G. Robinson, M. S. Sigman, M. S. Sanford, *J. Am. Chem. Soc.* **2019**, *141*, 15301–15306.
[26] C. Zhang, Y. Qian, Y. Ding, L. Zhang, X. Guo, Y. Zhao, G. Yu, *Angew. Chem.* **2019**, *131*, 7119–7124; *Angew. Chem. Int. Ed.* **2019**, *58*, 7045–7050.
[27] X. Xing, Q. Liu, W. Xu, W. Liang, J. Liu, B. Wang, J. P. Lemmon, *ACS Appl. Energ. Mater.* **2019**, *2*, 2364–2369.
[28] Y. Ding, C. Zhang, L. Zhang, Y. Zhou, G. Yu, *Chem* **2019**, *5*, 1964–1987.
[29] R. A. Potash, J. R. McKone, S. Conte, H. D. Abruña, *J. Electrochem. Soc.* **2015**, *163*, A338–A344.
[30] K. H. Hendriks, C. S. Sevov, M. E. Cook, M. S. Sanford, *ACS Energy Lett.* **2017**, *2*, 2430–2435.
[31] J. A. Kowalski, M. D. Casselman, A. P. Kaur, J. D. Milshtein, C. F. Elliott, S. Modekrutti, N. H. Attanayake, N. Zhang, S. R. Parkin, C. Risko, F. R. Brushett, S. A. Odom, *J. Mater. Chem. A* **2017**, *5*, 24371–24379.
[32] M. Milton, Q. Cheng, Y. Yang, C. Nuckolls, R. Hernández Sánchez, T. J. Sisto, *Nano Lett.* **2017**, *17*, 7859–7863.
[33] B. Hu, T. L. Liu, *J. Energy Chem.* **2018**, *27*, 1326–1332.
[34] G. Kwon, S. Lee, J. Hwang, H.-S. Shim, B. Lee, M. H. Lee, Y. Ko, S.-K. Jung, K. Ku, J. Hong, K. Kang, *Joule* **2018**, *2*, 1771–1782.
[35] J. Huang, Z. Yang, M. Vijayakumar, W. Duan, A. Hollas, B. Pan, W. Wang, X. Wei, L. A. Zhang, *Adv. Sustainable Syst.* **2018**, *2*, 1700131.
[36] G. Kwon, K. Lee, M. H. Lee, B. Lee, S. Lee, S.-K. Jung, K. Ku, J. Kim, S. Y. Park, J. E. Kwon, K. Kang, *Chem* **2019**, *5*, 2642–2656.
[37] N. H. Attanayake, J. A. Kowalski, K. V. Greco, M. D. Casselman, J. D. Milshtein, S. J. Chapman, S. R. Parkin, F. R. Brushett, S. A. Odom, *Chem. Mater.* **2019**, *31*, 4353–4363.
[38] S. G. Robinson, Y. Yan, K. H. Hendriks, M. S. Sanford, M. S. Sigman, *J. Am. Chem. Soc.* **2019**, *141*, 10171–10176.
[39] P. Geysens, Y. Li, I. Vankelecom, J. Fransaer, K. Binnemans, *ACS Sustainable Chem. Eng.* **2020**, *8*, 3832–3843.
[40] L. Zhang, Y. Qian, R. Feng, Y. Ding, X. Zu, C. Zhang, X. Guo, W. Wang, G. Yu, *Nat. Commun.* **2020**, *11*, 3843.
[41] J. D. Griffin, A. R. Pancoast, M. S. Sigman, *J. Am. Chem. Soc.* **2021**, *143*, 992–1004.
[42] Y. Yan, S. G. Robinson, T. P. Vaid, M. S. Sigman, M. S. Sanford, *J. Am. Chem. Soc.* **2021**, *143*, 13450–13459.
[43] Y. Yan, D. B. Vogt, T. P. Vaid, M. S. Sigman, M. S. Sanford, *Angew. Chem.* **2021**, *133*, 27245–27251.
[44] S. Ahn, J. H. Jang, J. Kang, M. Na, J. Seo, V. Singh, J. M. Joo, H. R. Byon, *ACS Energy Lett.* **2021**, *6*, 3390–3397.
[45] N. Daub, R. A. J. Janssen, K. H. Hendriks, *ACS Appl. Energ. Mater.* **2021**, *4*, 9248–9257.
[46] H. Chen, Z. Niu, J. Ye, C. Zhang, X. Zhang, Y. Zhao, *ACS Appl. Energ. Mater.* **2021**, *4*, 855–861.
[47] X. Fang, Z. Li, Y. Zhao, D. Yue, L. Zhang, X. Wei, *ACS Materials Lett.* **2022**, *4*, 277–306.
[48] R. M. Darling, K. G. Gallagher, J. A. Kowalski, S. Ha, F. R. Brushett, *Energy Environ. Sci.* **2014**, *7*, 3459–3477.
[49] F. Wudl, G. M. Smith, E. J. Hufnagel, *J. Chem. Soc. Chem. Commun.* **1970**, 1453–1454.
[50] Y. Chen, S. A. Freunberger, Z. Peng, O. Fontaine, P. G. Bruce, *Nat. Chem.* **2013**, *5*, 489–494.
[51] H.-D. Lim, B. Lee, Y. Zheng, J. Hong, J. Kim, H. Gwon, Y. Ko, M. Lee, K. Cho, K. Kang, *Nat. Energy* **2016**, *1*, 16066.
[52] Y. Fujihara, H. Kobayashi, S. Takaishi, T. Tomai, M. Yamashita, I. Honma, *ACS Appl. Mater. Interfaces* **2020**, *12*, 25748–25755.
[53] S. Iwamoto, Y. Inatomi, D. Ogi, S. Shibayama, Y. Murakami, M. Kato, K. Takahashi, K. Tanaka, N. Hojo, Y. Misaki, *Beilstein J. Org. Chem.* **2015**, *11*, 1136–1147.
[54] A. R. McNeill, S. E. Bodman, A. M. Burney, C. D. Hughes, D. L. Crittenden, *J. Phys. Chem. C* **2020**, *124*, 24105–24114.
[55] C. Wartelle, R. Viruela, P. M. Viruela, F. X. Sauvage, M. Sallé, E. Ortí, E. Levillain, F. Le Derf, *Phys. Chem. Chem. Phys.* **2003**, *5*, 4672–4679.
[56] B. Sudy, K. Rasmussen, G. Grampp *Mol. Phys.* **2014**, *113*, 1378–1385.
[57] R. P. Ashton, V. Balzani, J. Becher, A. Credi, M. C. T. Fyfe, G. Mattersteig, S. Menzer, M. B. Nielsen, F. M. Raymo, J. F. Stoddart, M. Venturi, D. J. Williams, *J. Am. Chem. Soc.* **1999**, *121*, 3951–3957.
[58] A. Ševčík, *Collect. Czech. Chem. Commun.* **1948**, *13*, 349–377.
[59] R. S. Nicholson, I. Shain, *Anal. Chem.* **1964**, *36*, 706–723.
[60] X. Wei, W. Duan, J. Huang, L. Zhang, B. Li, D. Reed, W. Xu, V. Sprenkle, W. Wang, *ACS Energy Lett.* **2016**, *1*, 705–711.
[61] C. Zhang, Y. Qian, Y. Ding, L. Zhang, X. Guo, Y. Zhao, G. Yu, *Angew. Chem.* **2019**, *131*, 7119–7124; *Angew. Chem. Int. Ed.* **2019**, *58*, 7045–7050.
[62] J. B. Torrance, B. A. Scott, B. Welber, F. B. Kaufman, P. E. Seiden, *Phys. Rev. B* **1979**, *19*, 730–741.
[63] S. V. Rosokha, J. K. Kochi, *J. Am. Chem. Soc.* **2007**, *129*, 828–838.
[64] V. Khodorkovsky, L. Shapiro, P. Krief, A. Shames, G. Mabon, A. Gorgues, M. Giffard, *Chem. Commun.* **2001**, 2736–2737.
[65] J.-F. Bergamini, P. Hapiot, D. Lorcy, *J. Electroanal. Chem.* **2006**, *593*, 87–98.
[66] P. Panda, D. Veldman, J. Sweelssen, J. J. A. M. Bastiaansen, B. M. W. Langeveld-Voss, S. C. J. Meskers, *J. Phys. Chem. B* **2007**, *111*, 5076–5081.

Manuscript received: August 30, 2022
Accepted manuscript online: September 13, 2022
Version of record online: October 25, 2022